8-2-2017

Drifts, currents, and power scrape-off width in SOLPS-ITER modeling of DIII-D

E. T. Meier
College of William and Mary, emeier@wm.edu

R. J. Goldston

E. G. Kaveeva

M. A. Makowski

S. Mordijck
College of William and Mary, smordijck@wm.edu

See next page for additional authors

Recommended Citation

Meier, E. T.; Goldston, R. J.; Kaveeva, E. G.; Makowski, M. A.; Mordijck, S.; Rozhansky, V. A.; Senichenkov, I. Yu.; and Voskoboynikov, S. P., Drifts, currents, and power scrape-off width in SOLPS-ITER modeling of DIII-D (2017). *NUCLEAR MATERIALS AND ENERGY*, 12.
10.1016/j.nme.2016.12.016

Nuclear Materials and Energy 12 (2017) 973–977

Contents lists available at ScienceDirect

Nuclear Materials and Energy

journal homepage: www.elsevier.com/locate/nme

Drifts, currents, and power scrape-off width in SOLPS-ITER modeling of DIII-D

E.T. Meier[a,*], R.J. Goldston[b], E.G. Kaveeva[c], M.A. Makowski[d], S. Mordijck[a], V.A. Rozhansky[c], I.Yu. Senichenkov[c], S.P. Voskoboynikov[c]

[a] College of William and Mary, Williamsburg, VA 23187, USA
[b] Princeton Plasma Physics Laboratory, Princeton, New Jersey 08540, USA
[c] Peter the Great St. Petersburg Polytechnic University, Polytechnicheskaya 29, 195251 St. Petersburg, Russia
[d] Lawrence Livermore National Laboratory, Livermore, California 94550, USA

ARTICLE INFO

Article history:
Received 15 July 2016
Revised 13 November 2016
Accepted 8 December 2016
Available online 27 December 2016

Keywords:
Power scrape-off width
SOLPS-ITER
Drift effects
SOL flows

ABSTRACT

The effects of drifts and associated flows and currents on the width of the parallel heat flux channel (λ_q) in the tokamak scrape-off layer (SOL) are analyzed using the SOLPS-ITER 2D fluid transport code. Motivation is supplied by Goldston's heuristic drift (HD) model for λ_q, which yields the same approximately inverse poloidal magnetic field dependence seen in multi-machine regression. The analysis, focusing on a DIII-D H-mode discharge, reveals HD-like features, including comparable density and temperature fall-off lengths in the SOL, and up-down ion pressure asymmetry that allows net cross-separatrix ion magnetic drift flux to exceed net anomalous ion flux. In experimentally relevant high-recycling cases, scans of both toroidal and poloidal magnetic field (B_{tor} and B_{pol}) are conducted, showing minimal λ_q dependence on either component of the field. Insensitivity to B_{tor} is expected, and suggests that SOLPS-ITER is effectively capturing some aspects of HD physics. Absence of λ_q dependence on B_{pol}, however, is inconsistent with both the HD model and experimental results. The inconsistency is attributed to strong variation in the parallel Mach number, which violates one of the premises of the HD model.

1. Introduction

Commercially viable fusion power generation depends on having reactors with infrequent and inexpensive maintenance. Given this goal, damage to tokamak plasma-facing components is a major concern, especially in the divertor region, where exhaust from the confined plasma is focused onto a narrow strip characterized by the so-called power scrape-off width, λ_q. Recent multi-tokamak regression analysis shows that λ_q has no size scaling, and approximately inverse scaling with poloidal magnetic field ($\sim B_{pol}^{-1}$), and predicts that ITER will have $\lambda_q \approx 1$ mm (mapped to the outer midplane) [1]. This is several times smaller than the previously estimated width of 4 mm, which assumed a significant positive effect on λ_q from the doubling of reactor major radius in going from today's largest machine, JET, to ITER. A reduced λ_q would tend to concentrate the 100 MW power exhaust in ITER, magnifying the already daunting challenge of spreading and dissipating power to achieve a tolerable target load of 10 MW/m^2.

Extrapolation to ITER based on empirical data entails uncertainty associated not only with the regression error bars — which indicate $\lambda_{q,ITER} \approx 0.7 - 1.1$ mm — but also with physical effects not represented in the database — such as detachment or modified SOL turbulence behavior in an ITER-size plasma. To mitigate risk, it is critical to develop the fullest possible theoretical understanding of the sensitivities of λ_q to B_{pol}, aspect ratio, overall size, and other tokamak parameters. A highly acknowledged theory, the heuristic drift (HD) model, closely reproduces the empirical scalings [2,3]. In the model, magnetic drifts drive plasma across flux surfaces at the drift speed during a characteristic scrape-off layer (SOL) dwell time set by half-sound-speed ($c_s/2$) parallel flows connecting the upstream plasma to the divertor target. (As used here and throughout the paper, "magnetic drifts" refers to the combined guiding-center grad B and curvature B drifts; notably, the divergence of these drifts is essentially identical to the divergence of the diamagnetic flux [4].) The drift speed multiplied by a chosen characteristic time establishes a density channel width; with an additional

* Corresponding author.
E-mail address: emeier@wm.edu (E.T. Meier).

http://dx.doi.org/10.1016/j.nme.2016.12.016

assumption that anomalous cross-field electron thermal transport heats the density channel, the HD model yields a prediction for λ_q. This 0D model, however, provides only generalized insight into the problem. Fluid modeling using a 2D transport code, as presented below, can supply additional insight. More sophisticated modeling that can capture kinetic and turbulence effects may be useful or even necessary to obtain a complete picture.

The analysis presented in this paper is a novel effort to apply fluid modeling, with drifts included, to study λ_q behavior in realistic high-recycling divertor conditions. A DIII-D discharge is used as the subject. An earlier paper has presented detailed results of similar modeling for low-recycling divertor conditions [5]. Low-recycling results are briefly summarized, and the focus is on high-recycling modeling.

2. Modeling setup

SOLPS-ITER [6,7] has been used to analyze a deuterium DIII-D H-mode discharge with 10 MW neutral beam input power, 1.5 MA plasma current, and toroidal magnetic field of −2 T (such that ion ∇B drift is toward the active X-point). Low-recycling and high-recycling scenarios are modeled. The plasma equations of SOLPS-ITER are based on those of Braginskii [8], but cross-field velocities are analytic, with terms that account for drifts [9,10] and parameterized turbulent transport. Neutral fluid modeling is used for the results presented here, though a more sophisticated and more computationally expensive Monte Carlo code, Eirene [11], is also available. Multi-charge-state impurity treatment and realistic sputtering models are also available. The neutral fluid modeling is favored in this case because the physics of the plasma model, especially the drift physics, is of primary interest for the attached divertor conditions modeled. Similarly, impurity effects are neglected in this modeling, improving computational tractability. For higher fidelity modeling, especially in situations with divertor detachment, the Monte Carlo neutral and detailed impurity modeling should be employed.

The grid used for low-recycling simulations is shown in Fig. 1(a). A simple orthogonal grid (not conforming to targets) is used. The core boundary is located 4.5 cm inside the outer midplane separatrix (at normalized poloidal flux $\psi_n = 0.85$). In all simulations, density at the core boundary is fixed to 4.5×10^{19} m^{-3}, and core boundary temperatures are fixed to $T_e = T_i = 500$ eV. Target recycling of 90% is used, primarily because the strong target pumping eliminates the need for tailored boundary conditions to achieve particle control. As a consequence of low recycling, the outer target plasma is sheath limited. Simulations are done for three cases: without drifts, with full drifts, and with

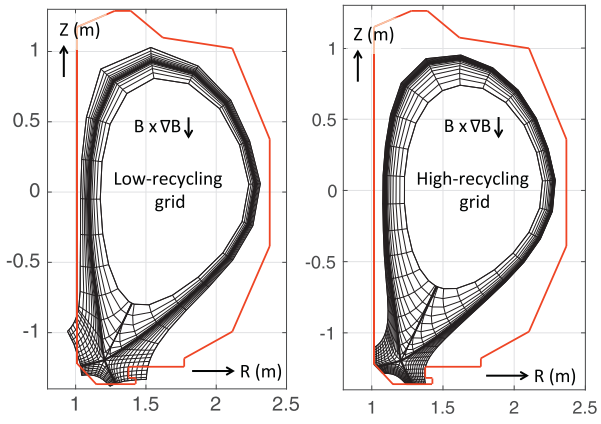

Fig. 1. Computational grids used for SOLPS-ITER analysis of DIII-D discharge 158,139 at 2850 ms, which had 10 MW neutral beam input power, and $I_p = 1.5$ MA.

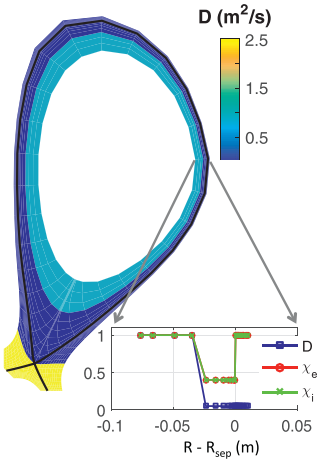

Fig. 2. Diffusivity profiles for "baseline" high-recycling simulation.

only magnetic drifts. Simulations "without drifts" do not include the magnetic (grad B plus curv B) or $E \times B$ drifts, but do include the other drifts [10], which are typically smaller; simulations with "full drifts" include all drifts; and simulations with "only magnetic drifts" exclude the $E \times B$ drift. Baseline simulations are established with particle diffusivity (D) and thermal diffusivities (χ_i and χ_e) set to 1 m^2/s everywhere in the domain except for the divertor region — no attempt is made to closely match upstream plasma profiles. Particle diffusivity in the SOL is scanned as described in Section 3.1. In the divertor region, all diffusivities are enhanced by a factor of five with respect to their SOL values, for numerical stability purposes.

In high-recycling simulations, the grid, boundary conditions, and diffusivities are adjusted to reproduce the upstream profiles of the H-mode plasma more accurately than was done in the low-recycling simulations. The grid is shown in Fig. 1(b). The core boundary is located 7.6 cm inside the outer midplane separatrix (at $\psi_n = 0.76$). In all simulations, density at the core boundary is fixed to 4.5×10^{19} m^{-3}, and core boundary temperatures are fixed to $T_e = T_i = 1000$ eV. At the targets, 100% recycling is used to represent complete saturation. The outermost flux surface of the grid corresponds to the location of the divertor cryopump duct, allowing particle control with the fluid neutral model. By specifying a small ion "leakage" rate, 0.1%, on this outer grid surface, pumping is approximated, allowing realistic particle control with high-recycling targets. Diffusivities have radial profiles, but are poloidally uniform, as shown in Fig. 2. χ_i and χ_e are 1 m^2/s in the core, and are reduced to 0.4 m^2/s in the pedestal region. The reduction of $\chi_{i,e}$ in the pedestal results in power input from the core boundary that is similar to the low-recycling simulations despite the higher core boundary temperatures. In the SOL and divertor regions, $\chi_i = \chi_e = 1$ and 20 m^2/s, respectively. D is 1 m^2/s in the inner core region, and is reduced to $D = 0.05$ m^2/s in the pedestal and SOL regions. In the divertor region, $D = 2.5$ m^2/s. The relatively high diffusivities in the divertor region facilitate numerical convergence, and capture experimentally realistic heat and particle spreading. Scans of poloidal and toroidal magnetic field strengths are conducted. All simulations have full drifts engaged.

3. Results and discussion

3.1. Low-recycling

For the three drift settings — no drifts, full drifts, and only magnetic drifts — particle diffusivity in the SOL (D_{SOL}) is scanned from 1 to 0.1 m^2/s. Reducing D_{SOL} below 0.1 m^2/s is not possible with

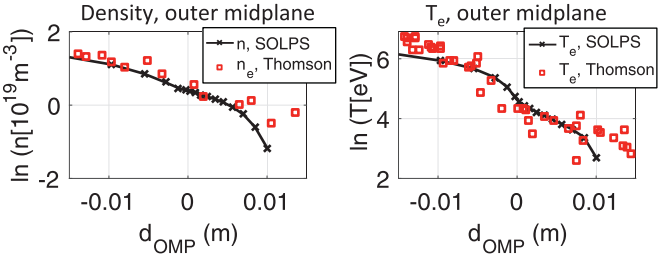

Fig. 3. Simulated and experimentally measured densities and temperatures as a function of outer miplane position relative to the separatrix. Density and temperature fall-off lengths are computed at $d_{OMP} = 2$ mm.

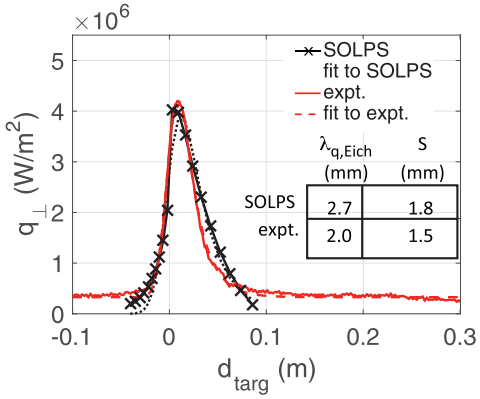

Fig. 4. Simulated and measured heat fluxes to outer target. Eich-style fits are shown in dotted lines. Eich spreading parameter, S, is given.

settings as described. Lower D_{SOL} could be achieved, hypothetically, by using higher divertor particle diffusivity or a modified scheme for smoothing the electrostatic potential as discussed in [5]. Two primary results are observed. First, simulations reach sufficiently low SOL diffusivity to be experimentally relevant. The SOL density fall-off length (L_n) decreases with D_{SOL} in all cases, and for $D_{SOL} = 0.1$ m^2/s, L_n values are comparable to the temperature fall-off lengths (L_{Te}), as found experimentally on AUG [12]. In the case with full drifts and $D_{SOL} = 0.1$ m^2/s, $L_n = 15$ mm and $L_{Te} = 7$ mm. Second, in both cases with magnetic drifts, L_n is enhanced as predicted by the HD model. At $D_{SOL} = 0.1$ m^2/s, $L_n = 7$ mm in the no-drift case, i.e., half of the full-drift value. Remarkably, this implies that as a result of drifts alone — without any particle diffusion! — the simulated density channel width will be consistent with observed widths on DIII-D and AUG.

Focusing on the full-drift case with $D_{SOL} = 0.1$ m^2/s, drifts are seen to impact the solution in several ways. Due to an in-out divertor target temperature asymmetry (which is absent in the no-drift case), the thermoelectric effect [13] generates a poloidal current carried primarily by electrons, which delivers nearly all of the deposited heat flux at the outer target, far exceeding the contribution from electron thermal conduction. Magnetic drifts exhibit the expected Pfirsch-Schlüter-like pattern in the SOL. Up-down ion pressure asymmetry produces net ion magnetic drift flux; such asymmetry and associated net flux are also seen in high-recycling simulations, and will be discussed in the context of those results in Section 3.2. As mentioned in the introduction, additional details of these low-recycling results are given in a separate publication [5].

While these low-recycling results provide insight into the role of drifts in the SOL, the simulations have features distinctly unlike the discharges studied in regression analysis [1]. For example, the low-recycling simulations have sheath-limited outer target conditions, with only 20% drop in T_e from outer midplane separatrix to outer strike point. The regression analysis focused on discharges with low-gas-puff conditions, but which had saturated, high-recycling targets, and significant drop in T_e along the SOL — that is, they were conduction-limited. Also, the dominant role of thermoelectric-driven heat flux in the simulations is probably the result of sheath-limited outer target conditions, and could cause SOL heat flux to behave differently than in a high-recycling scenario.

3.2. High-recycling

The high-recycling baseline solution closely matches the Thomson scattering data (from the shot and time indicated in the Fig. 1 caption) for density and temperature near the outer midplane separatrix as shown in Fig. 3. SOL gradient scale lengths, calculated at 2 mm outside of the outer midplane separatrix, are $L_n = 14$ mm and $L_{Te} = 8$ mm. The λ_q found in the simulation approximately matches the thermography-based heat flux measurement (again from the shot and time indicated in the Fig. 1 caption), see Fig. 4. The Gaussian spreading parameter, S, is similar to the DIII-D value, indicating that the chosen diffusivities provide realistic spreading. Outer target conditions are conduction-limited, and the inner target strike point is cool ($\sim$ 10 eV) with high density ($\sim 10^{20}$ m^{-3}). Note that the fitting technique developed by Eich et al. [14] is used to determine λ_q and S.

The SOL gradient ratio is $\eta_e = L_n/L_{Te} = 1.8$, similar to the value of 1.4 found on ASDEX Upgrade [12]. This implies that the chosen value of χ_e (1 m^2/s in the SOL) fills the density channel to an experimentally relevant extent. Sufficient anomalous electron transport to fill the density channel with energy is also assumed in the HD model [2]. Because L_{Te} is a proxy for λ_q— in the conduction-limited SOL, $\lambda_q \approx 2/7 L_{Te}$ [12,15,16] — λ_q is tied to L_n in the same way that L_{Te} is tied to L_n. When η_e is small, L_{Te} (and λ_q) should be relatively sensitive to χ_e. In contrast, when χ_e is high enough that $L_{Te} \to L_n$ (i.e., $\eta_e \approx 1$), the influence of χ_e on L_{Te} (and on λ_q) should be subdued; radial energy transport is proportional to density such that thermal energy cannot be driven beyond the density channel. In scans of magnetic field presented below, the expectation is that if η_e remains of order unity, the cross-field thermal transport is qualitatively valid. Theoretically, electron temperature gradient (ETG) microturbulence [17,18] could result in fixed η_e. In future work, it would be interesting to implement a critical gradient model that enhances χ_e when η_e exceeds an order-unity limit.

In the HD picture, some of the magnetic drift flux across the separatrix in the lower-outer quadrant is entrained in flow to the divertor. This entrained flux cannot participate in the Pfirsch-Schlüter circuit, and represents a net magnetic drift flux. In the original description of the HD model [2], an estimate of net magnetic drift flux was shown to be comparable to the net particle flux seen in DIII-D H-mode plasmas [19]. In the baseline high-recycling simulation, net ion magnetic drift flux across the separatrix is 3.0×10^{21} s^{-1}, while diffusive transport contributes 1.5×10^{21} s^{-1}. This simulated net cross-separatrix flux is comparable to experimental levels [19], capturing the surprising situation in which drift-driven cross-separatrix particle flux exceeds anomalous particle flux.

A simple classical drift picture will not permit net magnetic drift flux, due to the ambipolarity constraint, as pointed out in [20]. Magnetic drifts flux may be written as a pressure times an up-down-symmetric term proportional to $\mathbf{B} \times \nabla \mathbf{B}$, so the pressure itself must be up-down asymmetric to produce net drift flux. Such up-down asymmetry is indeed seen in the simulations. In the baseline high-recycling simulation, the ion pressure in the lower-outer quadrant is approximately 50% higher than the pressure at the top of the plasma, with density variation dominating the asymmetry, just as seen in low-recycling results described in detail in

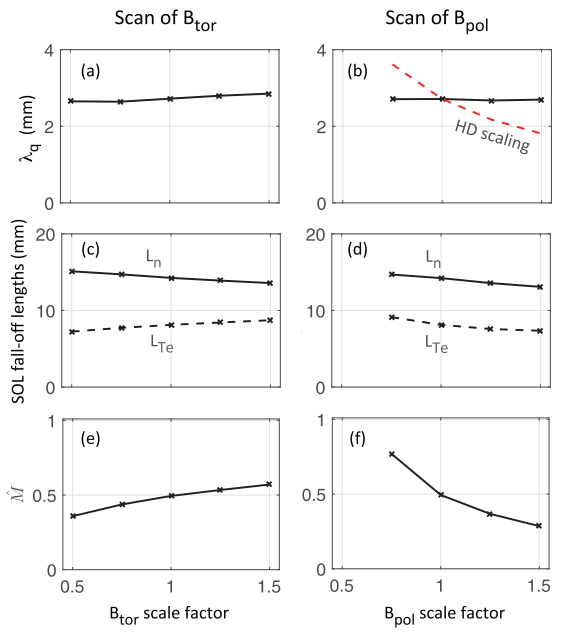

Fig. 5. Results of magnetic field scans. The effective Mach number ($\hat{M}$) is defined in the text. Insensitivity of λ_q to B_{tor} is expected. Strong variation of λ_q with B_{pol} is expected in the HD model, as shown in the dashed red line in panel (b), but is not seen in the simulation results. (For interpretation of the references to color in this figure legend, the reader is referred to the web version of this article.)

[5]. Electron and ion magnetic drifts are in opposite directions, resulting in net current (ion flux minus electron flux) due to magnetic drifts. Net current must be zero, but there is no other classical electron drift that can provide a non-ambipolar electron flux (since the $E \times B$ drift is ambipolar). As noted in [5], ambipolarity is enabled in SOLPS-ITER by artificially shifting an ion drift flux into the electron channel, but changing the direction of the flux such that the electrical current remains the same. Specifically, the perpendicular-viscosity-driven drift flux [5,10], is placed in the electron channel, allowing allows net cross-separatrix electron transport that matches the net ion transport. There is a risk that the artificial shift — the built-in default setting in the SOLPS-ITER package — could distort the physics picture. In future work, alternative non-ambipolar electron transport mechanisms, such as stochastic electron transport discussed by Goldston, could be explored with SOLPS-ITER.

A final noteworthy aspect of the baseline simulation is that thermoelectric-driven electron heat flux [13] contributes 50% of the peak heat flux deposition shown in Fig. 4. This result is consistent with the prediction of comparable electron conduction and convection in ITER L-mode conditions [21]. The presence of this convective heat flux does not cause an obvious deviation from the standard relationship for the conduction-limited SOL, $\lambda_q \approx 2/7 L_{Te}$, mentioned above, but such a possibility should be considered in future work. Experimental data supports the notion that thermoelectric-driven heat flux convection can be important [22,23], but additional experimental work is appropriate to validate computational results such as this one in which peak current density is 11 kA/m^2 near the outer strike point, and total current to the outer target is 4.0 kA.

As presented in Fig. 5(a,c,e), a scan of toroidal field strength from 50 to 150% of the nominal B_{tor} value results in $<$ 10% change of λ_q, and also modest changes in L_n and L_{Te}. In this scan, SOLPS-ITER seems to capture an essential feature of HD-predicted behavior: connection length ($L_{||}$) increases with B_{tor}, allowing more time (at a given parallel transport speed) for density channel broadening

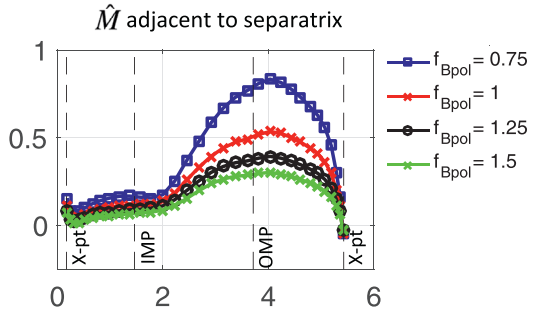

Fig. 6. Effective Mach number in the cells immediately outside the separatrix, plotted from X-point to X-point, passing the inner midplane (IMP) and outer midplane (OMP), for B_{pol} scale factor ranging from 0.75 to 1.5.

due to the dominant cross-field drift transport, but the drift speed is reduced with B_{tor}^{-1}, cancelling the connection length effect. In the HD model, a fundamental assumption is that the parallel particle transport is dictated by a flow at $c_s/2$, where c_s is the sound speed. A useful figure of merit for determining particle dwell time in the SOL is the effective Mach number,

$$\hat{M} \equiv \left(V_{||} + \frac{B}{B_{pol}} V_{pol} \right) / c_s, \tag{1}$$

where $V_{||}$ is the parallel flow speed, and V_{pol} is the poloidal projection of the combined drift velocities. The particle dwell time is then determined by $\tau_{||} = L_{||} (\hat{M} c_s)^{-1}$. In the scan of B_{tor}, $\hat{M}$ measured at the outer midplane separatrix exhibits small overall variation — a factor of 1.6 — as expected, given the absence of B_{tor} dependence in Pfirsch-Schlüter velocity, which is predicted to be

$$V_{||}^{PS} = \frac{2a}{R B_{pol}} \left(E_r - \frac{\nabla_r p_i}{en} \right), \tag{2}$$

in the large aspect ratio cylindrical approximation [15,24,25].

On the other hand, a similar scan of B_{pol}, results of which are shown in Fig. 5(b,d,f), reveals a surprising lack of λ_q variability. In the HD picture, as B_{pol} rises, the connection length is reduced, drift speeds are unchanged, and a reduction of SOL widths is expected. In the B_{pol} scan, however, $\hat{M}$ is reduced by nearly a factor of 3, breaking with the HD model, which assumes no change in $\hat{M}$. Based on Eq. (2), however, variation of $\hat{M}$ with B_{pol} is entirely expected. From this point of view, the fact that the SOLPS-ITER results are inconsistent with the HD picture is not a surprise. Examining $\hat{M}$ as a function of poloidal position in the row of cells adjacent to the separatrix, as shown in Fig. 6, reinforces the conclusions drawn from the outer midplane results. While $\hat{M}$ varies from a maximum at the midplane to zero at the X-point, the magnitude everywhere decreases with increasing B_{pol} as seen in Fig. 5(f). The sound speed is a weak function of B_{pol}: at the outer midplane separatrix, c_s is 1.3 $\times$ 10^5 m/s and 1.1 $\times$ 10^5 m/s for the weakest and strongest B_{pol} cases, respectively. An interesting implication of the simulation results, made clear in Fig. 6, is that magnetic drifts in the lower-outer quadrant compete with upward flow from the X-point to the outer midplane, opposite the direction assumed in the HD model derivation [2], which assumed $c_s/2$ flow toward the divertor. These results provide important motivation to identify SOL flow generation mechanisms that do not depend on B_{pol}, which may exist, but are missing from the SOLPS-ITER model.

4. Conclusions

SOLPS-ITER has been used to model a DIII-D H-mode discharge, with a focus on drift effects on λ_q. At sufficiently low SOL particle diffusivity, L_n in the SOL approaches the L_{Te}, resulting in $\eta_e \equiv L_n/L_{Te} \approx 1$ as seen experimentally. An up-down ion pressure

asymmetry results in net ion magnetic drift flux across the separatrix, with magnitude comparable to the experimentally observed cross-separatrix ion flux. Drifts contribute to a strong in-out asymmetry that drives a thermoelectric current such that electron convection contributes a significant fraction of the total power deposited on the outer target. In high-recycling simulations, experimental data, including outer midplane plasma profiles and heat flux deposition at the outer target, are well matched. In a scan of B_{tor}, λ_q exhibits minimal variation, consistent with experimental and theoretical expectations. On the other hand, the expected sensitivity of λ_q to B_{pol} is not found, apparently due to strong variation of the effective Mach number, which violates one of the premises of the HD model.

A variety of opportunities to improve the SOLPS-ITER modeling have been identified. Net ion magnetic drift flux is possible only because non-ambipolar electron transport is present. In this modeling, such transport is provided artificially by placing perpendicular-viscosity-driven ion drift flux in the electron channel. Stochastic electron transport could also serve this role, and should be considered in future efforts to validate SOLPS-ITER modeling. Results suggest that an adequate level of χ_e has been used in the simulations. However, a more physically meaningful approach, based on ETG microturbulence theory, could be used to raise χ_e when η_e exceeds a threshold value. Finally, by extending and validating modeling in partial and full detachment conditions, detachment effects on λ_q scaling behavior in ITER and other future devices can be addressed.

Acknowledgments

This work has been performed under U.S. Department of Energy Contract DE-SC0010434.

References

[1] T. Eich, et al., Nucl. Fusion 53 (2013) 093031.
[2] R.J. Goldston, Nucl. Fusion 52 (2012) 013009.
[3] R.J. Goldston, J. Nucl. Mater. 463 (2015) 397.
[4] A.V. Chankin, J. Nucl. Mater. 241 (1997) 199.
[5] E.T. Meier, et al., Plasma Phys. Control. Fusion 58 (2015) 125012.
[6] S. Wiesen, et al., J. Nucl. Mater. 463 (2015) 480.
[7] X. Bonnin, et al., Plasma Fusion Res. 11 (2016). 1403102
[8] S.I. Braginskii, Transport processes in a plasma, in: M.A. Leontovitch (Ed.), Reviews of Plasma Physics, Vol. 1, Consultants Bureau, New York, NY, 1965, pp. 205–311.
[9] V.A. Rozhansky, S.P. Voskoboynikov, E.G. Kaveeva, D.P. Coster, Simulation of tokamak edge plasmas including self-consistent electric fields, Nucl. Fusion 41 (2001) 387.
[10] V. Rozhansky, E. Kaveeva, P. Molchanov, I. Veselova, S. Voskoboynikov, D. Coster, G. Counsell, A. Kirk, S. Lisgo, the ASDEX-Upgrade Team and the MAST Team, Nucl. Fusion 49 (2009) 025007.
[11] D. Reiter, C. May, P. Borner, J. Nucl. Mater. 241 (1997) 342.
[12] H.J. Sun, et al., Plasma Phys. Control. Fusion 57 (2015) 125011.
[13] G.M. Staebler, F.L. Hinton, Nucl. Fusion 29 (1989) 1820.
[14] T. Eich, B. Sieglin, A. Scarabosio, W. Fundamenski, R. Goldston, A. Herrmann, Phys. Rev. Lett. 107 (2011) 215001.
[15] P.C. Stangeby, The Plasma Boundary of Magnetic Fusion Devices, IOP Publishing Ltd., 2000.
[16] M. Faitsch, et al., Plasma Phys. Control. Fusion 57 (2015) 075005.
[17] W. Dorland, et al., Phys. Rev. Lett. 85 (2000) 5579.
[18] F. Jenko, et al., Phys. Plasmas 16 (2009) 055901.
[19] G.D. Porter, DIII-D Team, Phys. Plasmas 5 (1998) 4311.
[20] A.V. Chankin, D.P. Coster, J. Nucl. Mater. 438 (2013) 463.
[21] V.A. Rozhansky, et al., in: in Proceedings of the 38th European Physical Society Conference on Plasma Physics, Strasbourg, France, 2011, p. P4.074.
[22] M. Komm, Private Commnication, 2016.
[23] A. Kallenbach, et al., J. Nucl. Mater. 290–293 (2001) 639.
[24] A.V. Chankin, et al., Nucl. Fusion 47 (2007) 762.
[25] J. Hugill, J. Nucl. Mater. 196 (1992) 918.